Simulating chiral spin liquids with projected entangled-pair states

Juraj Hasik,^{1,2} Maarten Van Damme,³ Didier Poilblanc,¹ and Laurens Vanderstraeten^{3,*}

Doubts have been raised on the representation of chiral spin liquids (CSL) exhibiting topological order in terms of projected entangled pair states (PEPS). Here, starting from a simple spin-1/2 chiral frustrated Heisenberg model, we show that a faithful representation of the CSL phase is in fact possible in terms of a generic PEPS upon variational optimization. We find a perfectly chiral gapless edge mode and a rapid decay of correlation functions at short distances consistent with a bulk gap, concomitant with a gossamer long-range tail originating from a PEPS bulk-edge correspondence. For increasing bond dimension, (i) the rapid decrease of spurious features – SU(2) symmetry breaking and long-range tails in correlations – together with (ii) a faster convergence of the ground state energy as compared to state-of-the-art cylinder-MPS simulations involving far more variational parameters, prove the fundamental relevance of the PEPS ansatz for simulating systems with chiral topological order.

Introduction— A chiral spin liquid (CSL) is a stronglycorrelated two-dimensional quantum spin system that serves as the lattice analog of a fractional quantum Hall (FQH) system [1–3]. The CSL is a disordered quantum state, and inherits many of the characteristic features of FQH physics, such as fractionalized excitations and protected chiral edge modes. The CSL was originally proposed on the level of a trial wavefunction, and later parent Hamiltonians were found [4–6] that stabilize such a wavefunction as its ground state. Although these are not expected to be found in real materials, in recent years many simpler model Hamiltonians were found that seem to realize CSL physics [7–18]. In these works, the use of performant numerical techniques such as variational matrix-product state (MPS) methods on cylindrical geometries, exact diagonalization on finite clusters or variational Monte-Carlo approaches were crucial for finding evidence of CSL features. Accurate numerical simulations are instrumental in relating theoretical descriptions of CSL physics to real materials that can be probed in experiments; for example, a few materials were found that realize the triangular-lattice Hubbard model [19–24], which possibly exhibits an emergent CSL phase between the metallic and the ordered insulating phase [25–27].

In recent years, projected entangled-pair states (PEPS) [28] have demonstrated a remarkable ability to simulate the ground states of strongly-correlated lattice systems in two dimensions [29–33]. This class of tensornetwork states can be formulated [34] and variationally optimized [35, 36] directly in the thermodynamic limit. The control parameters are the bond dimension D, controlling the amount of entanglement in the PEPS wavefunction, and the environment bond dimension χ , which is introduced when contracting the PEPS approximately with boundary MPS [28, 37, 38] or the corner-transfer

matrix renormalization group (CTMRG) [39–44]. When simulating a critical model, a variational PEPS wavefunction always exhibits a finite correlation length, which provides a length scale that can be used to extrapolate variational PEPS results [45–48]. In the case of non-chiral spin liquids, this procedure has proven very powerful [32].

The case of *chiral* systems is less straightforward: Whereas non-chiral topological order can be described by PEPS in a natural way [49-51] – for example, the RVB state on the kagome lattice is a simple example of gapped \mathbb{Z}_2 spin liquid and is written as a PEPS with bond dimension D=3 [52] – capturing a gapped chiral topological wavefunction seems to be a lot harder. The Gaussian fermionic PEPS wavefunctions that were proposed exhibit algebraic decay of correlations [53–55], a feature that was proven necessary for representing chiral free-fermionic states as PEPS [56], see also [57]. By Gutzwiller projecting two of these Gaussian PEPS, a CSL wavefunction can be constructed, exhibiting an entanglement spectrum with the degeneracy pattern of a chiral conformal field theory. Subsequently, a class of SU(2) invariant PEPS was proposed that exhibits chiral entanglement spectra [58–60]. Motivated by the properties of these trial wavefunctions, microscopic CSL Hamiltonians were successfully studied with PEPS, where both SU(2) and spatial symmetries were imposed on the PEPS tensors [61, 62]; recently, this approach was even extended to study SU(N) CSLs [33, 63]. In all these cases, however, the PEPS exhibits a decay of correlations slower than exponential, i.e. an *infinite* correlation length, which indicates an obstruction for simulating gapped chiral topological phases with PEPS, in line with the no-go theorem for the free-fermionic case. This, in turn, makes these types of simulations very challenging numerically, all of which has led to the view that PEPS are ill-suited for simulating chiral models.

In this paper, we want to disprove this view by performing an unconstrained PEPS simulation of an SU(2) CSL model on the square lattice. Comparing our results

¹Laboratoire de Physique Théorique, C.N.R.S. and Université de Toulouse, 31062 Toulouse, France

²Institute for Theoretical Physics, University of Amsterdam,

Science Park 904, 1098 XH Amsterdam, The Netherlands

³Department of Physics and Astronomy, University of Ghent, Krijgslaan 281, 9000 Gent, Belgium

^{*} Laurens.Vanderstraeten@ugent.be

with state-of-the-art MPS simulations on the cylinder, we find that the PEPS simulation provides very accurate results on the bulk properties *and* the topological edge properties of the CSL.

Model and methods— We investigate the model Hamiltonian

$$H = J_1 \sum_{\langle ij \rangle} \vec{S}_i \cdot \vec{S}_j + J_2 \sum_{\langle \langle ij \rangle \rangle} \vec{S}_i \cdot \vec{S}_j + i\lambda \sum_{\langle ijkl \rangle_p} \left(P_{ijkl} - P_{ijkl}^{-1} \right), \quad (1)$$

on an infinite square lattice, where \vec{S}_i are the spin-1/2 operators at site i, the first two sums are over nearest and next-nearest neighbours and the last sum is over all four-site plaquettes with P the cyclic permutation operator. This model was constructed by taking a long-ranged parent Hamiltonian [64] for the Kalmeyer-Laughlin state, and truncating the interaction terms [6]: it was shown numerically that the ground state stays in the same phase for a large choice of parameters. Note that the last term explicitly breaks the time-reversal and reflection symmetries separately, such that a CSL ground state is stabilized. Here, we take the parameters J_1 $2\cos(0.06\pi)\cos(0.14\pi)$, $J_2 = 2\cos(0.06\pi)\sin(0.14\pi)$ and $\lambda = 2\sin(0.06\pi)$, approximately identified as the point for which the ground state has maximal overlap with the Kalmeyer-Laughlin state [6]. This choice of parameters was also considered in Ref. 61, where a variational family of SU(2)-invariant PEPS was used.

A variational PEPS wavefunction can be represented as

parametrized by a single tensor A directly in the thermodynamic limit; the four virtual legs have bond dimension D and are contracted, whereas the physical legs correspond to the spins in the lattice. We impose rotation and reflection-conjugation symmetry on the tensor:

$$= -A , \qquad = -A . \qquad (3)$$

The tensor A can be optimized by a variational energy minimization; here, we use gradient optimization [36], where the energy is evaluated by CTMRG contraction and the energy gradient by automatic differentiation [65, 66]. The CTMRG contraction induces a second control parameter, the environment bond dimension χ . In our further calculations with the optimized PEPS, we use

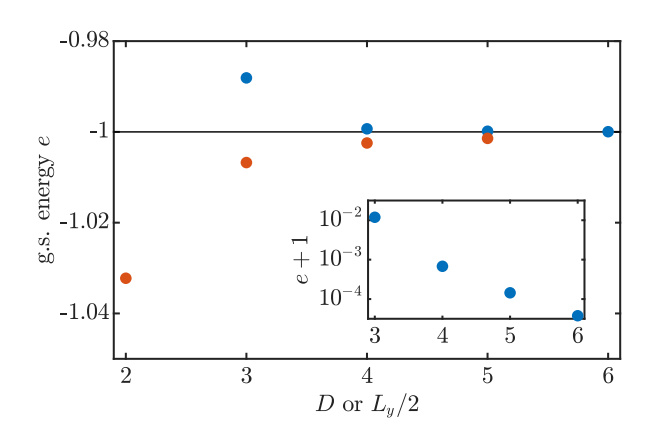


FIG. 1. **Energetics.** Main: The ground-state energy per site as a function of D (PEPS) or $L_y/2$ (cylinder-MPS). Inset: the variational PEPS energy compared to the value e=-1.

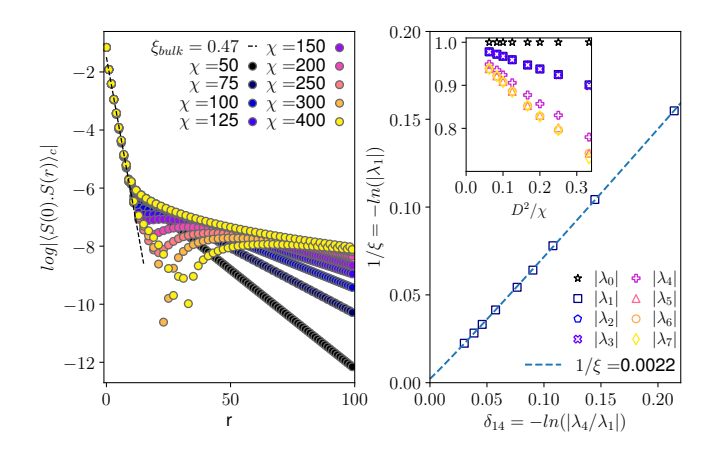


FIG. 2. Long-range properties of D=5 PEPS. Left: Connected part of the real space spin-spin correlation functions. Right: Scaling of correlation length by subleading gap $\delta_{14}=-log|\lambda_4/\lambda_1|$ in the transfer matrix E. The inset shows the leading part of the spectrum of E as a function of the environment dimension χ .

the CTMRG and VUMPS algorithms interchangeably for finding approximate environments, as these were recently shown to be equivalent [38].

Additionally, we simulate this model on infinite cylinders with circumference L_y using infinite MPS that are wound around the cylinder in a snake-like fashion. We have exploited SU(2) symmetry in the MPS simulation: because continuous symmetries necessarily remain unbroken on a finite- L_y cylinder, imposing this symmetry on the MPS is not a restriction. We use the variational uniform MPS (VUMPS) algorithm to find an optimal MPS approximation for the ground state [67, 68]. In our simulations, we go up to circumference $L_y = 10$; with a truncation error of $\epsilon = 10^{-5}$ we find that all reported observables have converged with a bond dimension (i.e., number of U(1) charges kept) around $D_{\rm MPS} = 15000$.

Bulk properties— Let us first look at the variational energies that are obtained with both methods. In Fig. 1

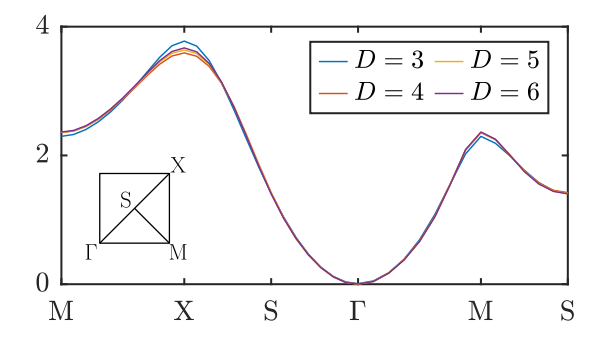


FIG. 3. Static structure factor. The momentum-resolved correlation function [Eq. (6)] for the D=5 PEPS for a path through the Brillouin zone.

we plot the ground-state energies. For D = 4, we find a significantly better value of the energy than the SU(2)-invariant PEPS with the same bond dimension [61]. As the inset shows, the variational energy converges exponentially with D, which is in stark contrast with PEPS approximations for critical models, where a power-law extrapolation with the correlation length is typically needed. We have also plotted the energy density as obtained from the cylinder-MPS simulations, where the finite circumference leads to an undershooting of the energy. From this comparison, it is clear that PEPS give more accurate values for the ground-state energy than the cylinder-MPS approach – certainly given the fact that the largest MPS in our simulations contains around 70 million variational parameters (encorporating the SU(2)symmetry), compared to only around 2600 for the D=6PEPS.

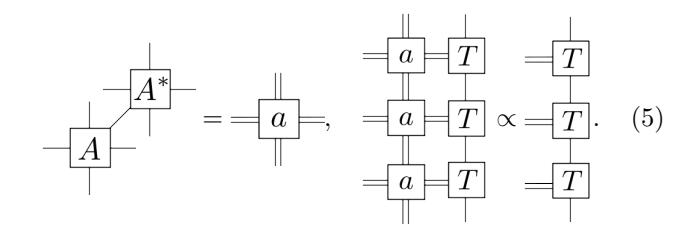
Surprisingly, we find that the energy converges to the value of e = -1. Given that the parameters in the model were not fine-tuned or chosen in a natural way, this feature is really peculiar and we did not find any satisfying explanation for this observation.

Let us then look at the magnetization. In PEPS simulations of models close to criticality, order parameters are typically overestimated due to finite-D effects, and a proper scaling of the order parameter is needed to get accurate results. Here, however, we find surprisingly small values of the magnetization already for small D: for D=3 we find a magnetization of $m=10^{-3}$, which further decrease down to $m\approx 10^{-5}$ at D=6.

Next, in Fig. 2 we have plotted the structure of the correlations in the PEPS. The spin-spin correlation function along a horizontal row in the lattice is determined by the spectrum of the transfer matrix E [69, 70],

where a is a double-layer tensor with bond dimension D^2

and T defines the boundary MPS approximation of the leading eigenvector of the PEPS transfer matrix



We plot the leading eigenvalues of E in Fig. 2 (right panel) for the D=5 PEPS and increasing values of χ . We observe that the gap in the transfer matrix approaches zero, indicating that the correlation length diverges. This is confirmed by the scaling of the correlation length to the infinite- χ limit; we find a correlation length of, at least, 450 sites. When plotting the spin-spin correlation function, however, we find an extended regime of exponential decay with a correlation length $\xi_{\rm bulk}=0.47$, and an algebraic decay with a magnitude of order 10^{-7} . This indicates that the part of the transfer matrix with diverging correlation length gives only a very small contribution to the spin-spin correlations. For comparison we perform a similar analysis on a D=3 SU(2)-invariant PEPS in the Appendix.

Finally, we examine the momentum-resolved structure factor,

$$s(q_x, q_y) = \sum_{mn} e^{i(q_x m + q_y n)} \langle \vec{S}_{mn} \cdot \vec{S}_{00} \rangle, \qquad (6)$$

which we evaluate using the methods from Ref. 38. We plot this quantity through a path of the Brillouin zone for different PEPS bond dimensions, showing a smooth behaviour at the X point and a vanishing at the Γ point – exactly what one would expect for a gapped spin liquid. In addition, the curve has nicely converged as a function of PEPS bond dimension D. Note that this is the first instance where a spin liquid for spin-1/2 system on a square lattice was found numerically by single-site PEPS, without imposing the SU(2) symmetry explicitly.

Entanglement spectrum— As one of the defining characteristics of a chiral topological phase, we now investigate the entanglement spectrum of our variational PEPS ground states. Following the PEPS bulk-boundary correspondence [71], the entanglement Hamiltonian $H_{\rm ent}$ can be inferred directly from the fixed-point ρ of the PEPS transfer matrix of Eq. (5) as $\rho = {\rm e}^{-H_{\rm ent}}$. Numerically, we take the boundary MPS with bond dimension χ , fold it open and interpret it as a matrix-product operator (MPO) approximation for ρ . We have found above that ρ has infinite correlation length in the infinite- χ limit, suggesting that $H_{\rm ent}$ has long-range interaction terms. Indeed, a thermal density operator for a local or exponentially-decaying Hamiltonian could be efficiently represented as an MPO with finite bond dimension [72].

First we compute the low-lying spectrum of $H_{\rm ent}$ for the infinite system: we first find the leading eigenvector of ρ as an infinite MPS with the VUMPS algorithm, and then apply a variational excitation ansatz with fixed momentum to capture the excited states of ρ [68, 73]. A third control parameter enters here, the bond dimension χ' of this infinite MPS. In Fig. 4 we plot the results of this procedure for the D=5 PEPS. The lower-left panel shows the typical sawtooth form of a chiral spectrum in the full Brillouin zone, but the zoomed spectrum in the top panel around the origin shows that we also find a very steep mode. As the bottom-right panel shows, this additional mode gets steeper as the MPO's bond dimension χ is increased. This finding agrees with the fact that at finite χ the MPO has finite correlation length, and that H_{ent} is not truly long-range; therefore, the spectrum cannot be perfectly chiral [74] at finite χ . Only in the infinite- χ limit we expect to find a perfectly chiral entanglement spectrum.

Second, we compute the entanglement spectrum on a finite system of N sites with periodic boundary conditions by placing the MPO approximation for ρ on a finite ring. Since computing the spectrum exactly scales as $\mathcal{O}(D^N)$, it becomes quickly unfeasible for large D or N. As an alternative, we use open-boundary MPS methods for finding the low-lying spectrum of MPOs on a ring [75]; here, again, the bond dimension χ' enters as a control parameter. In Fig. 5 we show the entanglement spectrum of the D = 5 PEPS confined on rings of different sizes, clearly showing the chiral branch with the degeneracies that are expected for the $SU(2)_1$ Wess-Zumino-Witten conformal field theory. Moreover, we find the degeneracies of the SU(2) multiplets, again indicating that the PEPS is an SU(2)-invariant state up to high precision. In the left panel, we compare the spectra with the entanglement spectra as obtained from the MPS ground states on the cylinder; here, we use the usual prescription [76] for assigning momentum quantum numbers to the MPS entanglement spectrum. The two figures agree nicely, but the PEPS methodology allows us to reach much larger system sizes with moderate computational cost.

Conclusions— This work shows that CSLs exhibiting topological order can be represented faithfully in terms of generic bosonic PEPS upon variational optimization. The suspicion of an obstruction [56] stems directly from the PEPS bulk-edge correspondence: the existence of a perfectly gapless chiral edge mode implies that the (onedimensional) entanglement Hamiltonian [52, 71] is longrange which, in turn, implies an infinite correlation length in the bulk. Nevertheless, our work shows that this feature does not prohibit us from variationally optimizing these PEPS efficiently, and that the divergence of the correlation length is connected to an irrelevant vanishing long-range tail in some correlation functions. The rapid exponential convergence of the energy (much faster than the convergence of cylinder-MPS with circumference) and the vanishing of the magnetization are consistent with the expected bulk gap.

Although the case of an SU(2) Abelian CSL is considered here, we believe that chiral PEPS can more

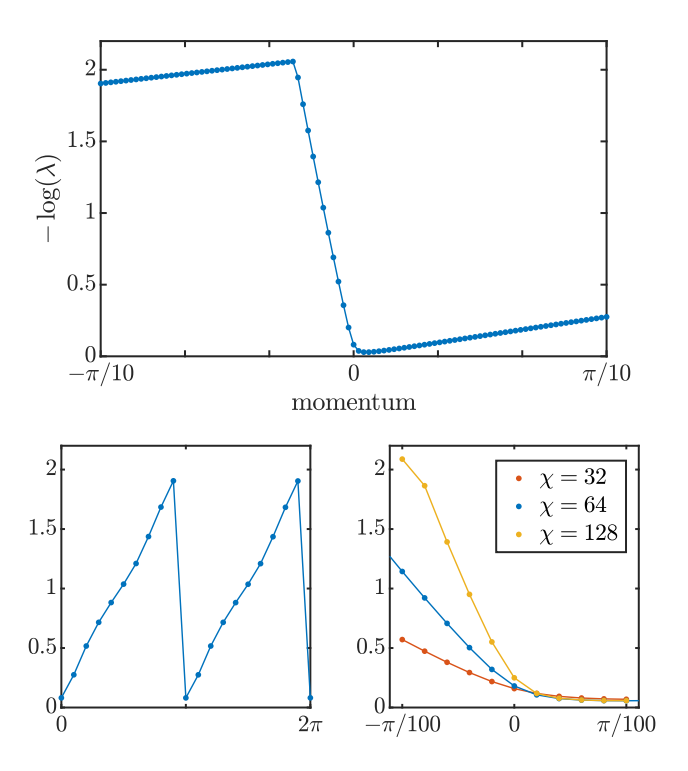


FIG. 4. Entanglement spectrum in thermodynamic limit. We show results for the entanglement spectrum of the D=5 PEPS, using the quasiparticle ansatz. (Top) A close-up for momenta around the origin, evaluated with $\chi=64$ and $\chi'=128$, nicely showing the two branches. (Left) The dispersion in the full Brillouin zone. (Right) An even narrower close-up around the origin for three different values of χ and $\chi'=128$.

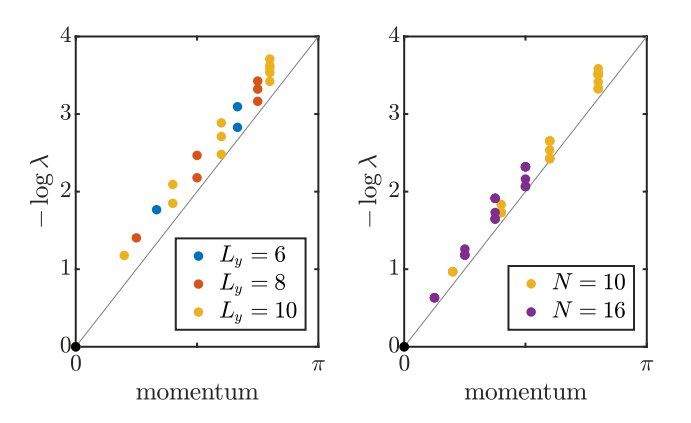


FIG. 5. Entanglement spectrum for finite system. (Left) Cylinder-MPS results for three different L_y . (Right) Spectrum of the MPO representation for the entanglement Hamiltonian ρ confined on a ring of two different sizes N, as computed with the method in Ref. 75 with $\chi=32$ and $\chi'=80$. Here we show the four first values of the momentum. We do not show the degeneracies of the SU(2) multiplets (for the cylinder-MPS these are exact, for the PEPS we find degeneracies up to the third or fourth digit).

broadly faithfully represent Abelian and non-Abelian SU(N) CSL, $N \geq 2$, as suggested by calculations involving spin-symmetric PEPS [33, 62]. We can also tackle cases of bosonic fractional Chern insulators such as the Harper-Hofstadter model [77], which can be realized in atomic simulators [78, 79]. Finally, we are convinced that fermionic PEPS [80, 81] would be extremely well suited to describe electronic systems with chiral topological order like interacting Chern insulators at fractional fill-

ing [82, 83] or chiral spin liquids close to a metal-insulator transition [25-27].

Acknowledgments— We acknowledge inspiring discussions with Norbert Schuch and Frank Verstraete. This work was supported by the Research Foundation Flanders. D. P. acknowledges support by the TNTOP ANR-18-CE30-0026-01 grant awarded by the French Research Council. This work was granted access to the HPC resources of CALMIP center under the allocation 2017-P1231.

- V. Kalmeyer and R. B. Laughlin, Equivalence of the resonating-valence-bond and fractional quantum hall states, Phys. Rev. Lett. 59, 2095 (1987).
- [2] V. Kalmeyer and R. B. Laughlin, Theory of the spin liquid state of the heisenberg antiferromagnet, Phys. Rev. B 39, 11879 (1989).
- [3] X. G. Wen, F. Wilczek, and A. Zee, Chiral spin states and superconductivity, Phys. Rev. B 39, 11413 (1989).
- [4] D. F. Schroeter, E. Kapit, R. Thomale, and M. Greiter, Spin hamiltonian for which the chiral spin liquid is the exact ground state, Phys. Rev. Lett. 99, 097202 (2007).
- [5] R. Thomale, E. Kapit, D. F. Schroeter, and M. Greiter, Parent hamiltonian for the chiral spin liquid, Phys. Rev. B 80, 104406 (2009).
- [6] A. E. Nielsen, G. Sierra, and J. I. Cirac, Local models of fractional quantum hall states in lattices and physical implementation, Nat. Comm. 4, 2864 (2013).
- [7] L. Messio, B. Bernu, and C. Lhuillier, Kagome antiferromagnet: A chiral topological spin liquid?, Phys. Rev. Lett. 108, 207204 (2012).
- [8] B. Bauer, L. Cincio, B. P. Keller, M. Dolfi, G. Vidal, S. Trebst, and A. W. Ludwig, Chiral spin liquid and emergent anyons in a kagome lattice mott insulator, Nature communications 5, 1 (2014).
- [9] S.-S. Gong, W. Zhu, and D. Sheng, Emergent chiral spin liquid: Fractional quantum hall effect in a kagome heisenberg model, Scientific reports 4, 1 (2014).
- [10] Y.-C. He, D. N. Sheng, and Y. Chen, Chiral spin liquid in a frustrated anisotropic kagome heisenberg model, Phys. Rev. Lett. 112, 137202 (2014).
- [11] W.-J. Hu, W. Zhu, Y. Zhang, S. Gong, F. Becca, and D. N. Sheng, Variational monte carlo study of a chiral spin liquid in the extended heisenberg model on the kagome lattice, Phys. Rev. B 91, 041124 (2015).
- [12] S.-S. Gong, W. Zhu, L. Balents, and D. N. Sheng, Global phase diagram of competing ordered and quantum spinliquid phases on the kagome lattice, Phys. Rev. B 91, 075112 (2015).
- [13] A. Wietek, A. Sterdyniak, and A. M. Läuchli, Nature of chiral spin liquids on the kagome lattice, Phys. Rev. B 92, 125122 (2015).
- [14] A. Wietek and A. M. Läuchli, Chiral spin liquid and quantum criticality in extended $s=\frac{1}{2}$ heisenberg models on the triangular lattice, Phys. Rev. B **95**, 035141 (2017).
- [15] C. Hickey, L. Cincio, Z. Papić, and A. Paramekanti, Emergence of chiral spin liquids via quantum melting of noncoplanar magnetic orders, Phys. Rev. B 96, 115115 (2017).

- [16] S.-S. Gong, W. Zhu, J.-X. Zhu, D. N. Sheng, and K. Yang, Global phase diagram and quantum spin liquids in a spin-½ triangular antiferromagnet, Phys. Rev. B 96, 075116 (2017).
- [17] A. Szasz, J. Motruk, M. P. Zaletel, and J. E. Moore, Chiral spin liquid phase of the triangular lattice hubbard model: A density matrix renormalization group study, Phys. Rev. X 10, 021042 (2020).
- [18] T. Cookmeyer, J. Motruk, and J. E. Moore, Four-spin terms and the origin of the chiral spin liquid in mott insulators on the triangular lattice, Phys. Rev. Lett. 127, 087201 (2021).
- [19] Y. Shimizu, K. Miyagawa, K. Kanoda, M. Maesato, and G. Saito, Spin liquid state in an organic mott insulator with a triangular lattice, Phys. Rev. Lett. 91, 107001 (2003).
- [20] T. Itou, A. Oyamada, S. Maegawa, M. Tamura, and R. Kato, Spin-liquid state in an organic spin-1/2 system on a triangular lattice, EtMe₃Sb[Pd(dmit)₂]₂, Journal of Physics: Condensed Matter 19, 145247 (2007).
- [21] K. T. Law and P. A. Lee, 1t-tas2 as a quantum spin liquid, Proceedings of the National Academy of Sciences 114, 6996 (2017).
- [22] J. M. Ni, B. L. Pan, B. Q. Song, Y. Y. Huang, J. Y. Zeng, Y. J. Yu, E. J. Cheng, L. S. Wang, D. Z. Dai, R. Kato, and S. Y. Li, Absence of Magnetic Thermal Conductivity in the Quantum Spin Liquid Candidate EtMe₃Sb[Pd(dmit)₂]₂, Phys. Rev. Lett. 123, 247204 (2019).
- [23] B. Miksch, A. Pustogow, M. J. Rahim, A. A. Bardin, K. Kanoda, J. A. Schlueter, R. Hübner, M. Scheffler, and M. Dressel, Gapped magnetic ground state in quantum spin liquid candidate κ-(BEDT – TTF₂)Cu₂(CN₃), Science 372, 276 (2021).
- [24] W. Ruan, Y. Chen, S. Tang, J. Hwang, H.-Z. Tsai, R. L. Lee, M. Wu, H. Ryu, S. Kahn, F. Liou, et al., Evidence for quantum spin liquid behaviour in single-layer 1t-tase2 from scanning tunnelling microscopy, Nature Physics 17, 1154 (2021).
- [25] A. Szasz, J. Motruk, M. P. Zaletel, and J. E. Moore, Chiral spin liquid phase of the triangular lattice hubbard model: A density matrix renormalization group study, Phys. Rev. X 10, 021042 (2020).
- [26] B.-B. Chen, Z. Chen, S.-S. Gong, D. N. Sheng, W. Li, and A. Weichselbaum, Quantum spin liquid with emergent chiral order in the triangular-lattice hubbard model, arXiv:2102.05560 (2021).
- [27] L. F. Tocchio, A. Montorsi, and F. Becca, Hubbard model

- on triangular *n*-leg cylinders: Chiral and nonchiral spin liquids, Phys. Rev. Research **3**, 043082 (2021).
- [28] F. Verstraete and J. I. Cirac, Renormalization algorithms for quantum-many body systems in two and higher dimensions, arXiv:cond-mat/04070663 (2004).
- [29] P. Corboz and F. Mila, Tensor network study of the shastry-sutherland model in zero magnetic field, Phys. Rev. B 87, 115144 (2013).
- [30] P. Corboz, T. M. Rice, and M. Troyer, Competing States in the t-J Model: Uniform d-Wave State versus Stripe State (Supplemental Material), Phys. Rev. Lett. 113, 046402 (2014).
- [31] B.-X. Zheng, C.-M. Chung, P. Corboz, G. Ehlers, M.-P. Qin, R. M. Noack, H. Shi, S. R. White, S. Zhang, and G. K.-L. Chan, Stripe order in the underdoped region of the two-dimensional hubbard model, Science 358, 1155 (2017).
- [32] J. Hasik, D. Poilblanc, and F. Becca, Investigation of the Néel phase of the frustrated Heisenberg antiferromagnet by differentiable symmetric tensor networks, SciPost Phys. 10, 12 (2021).
- [33] J.-Y. Chen, J.-W. Li, P. Nataf, S. Capponi, M. Mambrini, K. Totsuka, H.-H. Tu, A. Weichselbaum, J. von Delft, and D. Poilblanc, Abelian su(n)₁ chiral spin liquids on the square lattice, Phys. Rev. B 104, 235104 (2021).
- [34] J. Jordan, R. Orús, G. Vidal, F. Verstraete, and J. I. Cirac, Classical simulation of infinite-size quantum lattice systems in two spatial dimensions, Phys. Rev. Lett. 101, 250602 (2008).
- [35] P. Corboz, Variational optimization with infinite projected entangled-pair states, Phys. Rev. B 94, 035133 (2016).
- [36] L. Vanderstraeten, J. Haegeman, P. Corboz, and F. Verstraete, Gradient methods for variational optimization of projected entangled-pair states, Phys. Rev. B 94, 155123 (2016).
- [37] M. T. Fishman, L. Vanderstraeten, V. Zauner-Stauber, J. Haegeman, and F. Verstraete, Faster methods for contracting infinite two-dimensional tensor networks, Phys. Rev. B 98, 235148 (2018).
- [38] L. Vanderstraeten, L. Burgelman, B. Ponsioen, M. V. Damme, B. Vanhecke, P. Corboz, J. Haegeman, and F. Verstraete, Variational methods for contracting projected entangled-pair states, arXiv:2110.12726 (2021).
- [39] R. J. Baxter, Dimers on a rectangular lattice, J. Math. Phys. 9, 650 (1968).
- [40] R. J. Baxter, Variational approximations for square lattice models in statistical mechanics, J. Stat. Phys. 19, 461 (1978).
- [41] T. Nishino and K. Okunishi, Corner transfer matrix renormalization group method, J. Phys. Soc. Jap. 65, 891 (1996).
- [42] T. Nishino and K. Okunishi, Corner transfer matrix algorithm for classical renormalization group, J. Phys. Soc. Jap. 66, 3040 (1997).
- [43] R. Orús and G. Vidal, Simulation of two-dimensional quantum systems on an infinite lattice revisited: Corner transfer matrix for tensor contraction, Phys. Rev. B 80, 094403 (2009).
- [44] P. Corboz, J. Jordan, and G. Vidal, Simulation of fermionic lattice models in two dimensions with projected entangled-pair states: Next-nearest neighbor hamiltonians, Phys. Rev. B 82, 245119 (2010).
- [45] P. Corboz, P. Czarnik, G. Kapteijns, and L. Tagliacozzo,

- Finite Correlation Length Scaling with Infinite Projected Entangled-Pair States, Phys. Rev. X 8, 031031 (2018).
- [46] M. Rader and A. M. Läuchli, Finite Correlation Length Scaling in Lorentz-Invariant Gapless iPEPS Wave Functions, Phys. Rev. X 8, 031030 (2018).
- [47] P. Czarnik and P. Corboz, Finite correlation length scaling with infinite projected entangled pair states at finite temperature, Phys. Rev. B 99, 245107 (2019).
- [48] B. Vanhecke, J. Hasik, F. Verstraete, and L. Vanderstraeten, A scaling hypothesis for projected entangledpair states, arXiv:2102.03143 (2021).
- [49] N. Schuch, I. Cirac, and D. Pérez-García, Peps as ground states: Degeneracy and topology, Annals of Physics 325, 2153 (2010).
- [50] N. Schuch, D. Pérez-García, and I. Cirac, Classifying quantum phases using matrix product states and projected entangled pair states, Phys. Rev. B 84, 165139 (2011).
- [51] M. B. Şahinoğlu, D. Williamson, N. Bultinck, M. Mariën, J. Haegeman, N. Schuch, and F. Verstraete, Characterizing topological order with matrix product operators, in *Annales Henri Poincaré*, Vol. 22 (Springer, 2021) pp. 563–592.
- [52] D. Poilblanc, N. Schuch, D. Pérez-García, and J. I. Cirac, Topological and entanglement properties of resonating valence bond wave functions, Phys. Rev. B 86, 014404 (2012).
- [53] T. B. Wahl, H.-H. Tu, N. Schuch, and J. I. Cirac, Projected entangled-pair states can describe chiral topological states, Phys. Rev. Lett. 111, 236805 (2013).
- [54] T. B. Wahl, S. T. Haßler, H.-H. Tu, J. I. Cirac, and N. Schuch, Symmetries and boundary theories for chiral projected entangled pair states, Phys. Rev. B 90, 115133 (2014).
- [55] Q. Mortier, N. Schuch, F. Verstraete, and J. Haegeman, Tensor networks can resolve Fermi surfaces, arXiv:2008.11176 (2020).
- [56] J. Dubail and N. Read, Tensor network trial states for chiral topological phases in two dimensions and a nogo theorem in any dimension, Phys. Rev. B 92, 205307 (2015).
- [57] A. Kapustin and L. Fidkowski, Local commuting projector hamiltonians and the quantum hall effect, Communications in Mathematical Physics 373, 763 (2020).
- [58] D. Poilblanc, J. I. Cirac, and N. Schuch, Chiral topological spin liquids with projected entangled pair states, Phys. Rev. B 91, 224431 (2015).
- [59] D. Poilblanc, N. Schuch, and I. Affleck, $SU(2)_1$ chiral edge modes of a critical spin liquid, Phys. Rev. B **93**, 174414 (2016).
- [60] A. Hackenbroich, A. Sterdyniak, and N. Schuch, Interplay of su(2), point group, and translational symmetry for projected entangled pair states: Application to a chiral spin liquid, Phys. Rev. B 98, 085151 (2018).
- [61] D. Poilblanc, Investigation of the chiral antiferromagnetic heisenberg model using projected entangled pair states, Phys. Rev. B 96, 121118 (2017).
- [62] J.-Y. Chen, L. Vanderstraeten, S. Capponi, and D. Poilblanc, Non-abelian chiral spin liquid in a quantum antiferromagnet revealed by an ipeps study, Phys. Rev. B 98, 184409 (2018).
- [63] J.-Y. Chen, S. Capponi, A. Wietek, M. Mambrini, N. Schuch, and D. Poilblanc, SU(3)₁ chiral spin liquid on the square lattice: A view from symmetric projected en-

- tangled pair states, Phys. Rev. Lett. 125, 017201 (2020).
- [64] A. E. B. Nielsen, J. I. Cirac, and G. Sierra, Laughlin spinliquid states on lattices obtained from conformal field theory, Phys. Rev. Lett. 108, 257206 (2012).
- [65] H.-J. Liao, J.-G. Liu, L. Wang, and T. Xiang, Differentiable programming tensor networks, Phys. Rev. X 9, 031041 (2019).
- [66] J. Hasik and G. B. Mbeng, peps-torch: A differentiable tensor network library for two-dimensional lattice models, https://github.com/jurajHasik/peps-torch.
- [67] V. Zauner-Stauber, L. Vanderstraeten, M. T. Fishman, F. Verstraete, and J. Haegeman, Variational optimization algorithms for uniform matrix product states, Phys. Rev. B 97, 045145 (2018).
- [68] L. Vanderstraeten, J. Haegeman, and F. Verstraete, Tangent-space methods for uniform matrix product states, SciPost Phys. Lect. Notes, 7 (2019).
- [69] T. Nishino, K. Okunishi, and M. Kikuchi, Numerical renormalization group at criticality, Physics Letters A 213, 69 (1996).
- [70] M. M. Rams, P. Czarnik, and L. Cincio, Precise extrapolation of the correlation function asymptotics in uniform tensor network states with application to the bosehubbard and xxz models, Phys. Rev. X 8, 041033 (2018).
- [71] J. I. Cirac, D. Poilblanc, N. Schuch, and F. Verstraete, Entanglement spectrum and boundary theories with projected entangled-pair states, Phys. Rev. B 83, 245134 (2011).
- [72] A. Molnar, N. Schuch, F. Verstraete, and J. I. Cirac, Approximating gibbs states of local hamiltonians efficiently with projected entangled pair states, Phys. Rev. B 91, 045138 (2015).
- [73] J. Haegeman and F. Verstraete, Diagonalizing transfer matrices and matrix product operators: A medley of exact and computational methods, Ann. Rev. Cond. Mat. Phys. 8, 355 (2017).
- [74] H. Nielsen and M. Ninomiya, A no-go theorem for regularizing chiral fermions, Physics Letters B 105, 219 (1981).
- [75] M. Van Damme, R. Vanhove, J. Haegeman, F. Verstraete, and L. Vanderstraeten, Efficient matrix product state methods for extracting spectral information on rings and cylinders, Phys. Rev. B 104, 115142 (2021).
- [76] L. Cincio and G. Vidal, Characterizing topological order by studying the ground states on an infinite cylinder, Phys. Rev. Lett. 110, 067208 (2013).
- [77] A. S. Sørensen, E. Demler, and M. D. Lukin, Fractional quantum hall states of atoms in optical lattices, Phys. Rev. Lett. 94, 086803 (2005).
- [78] M. Aidelsburger, M. Atala, M. Lohse, J. T. Barreiro, B. Paredes, and I. Bloch, Realization of the hofstadter hamiltonian with ultracold atoms in optical lattices, Phys. Rev. Lett. 111, 185301 (2013).
- [79] H. Miyake, G. A. Siviloglou, C. J. Kennedy, W. C. Burton, and W. Ketterle, Realizing the harper hamiltonian with laser-assisted tunneling in optical lattices, Phys. Rev. Lett. 111, 185302 (2013).
- [80] C. V. Kraus, N. Schuch, F. Verstraete, and J. I. Cirac, Fermionic projected entangled pair states, Phys. Rev. A 81, 052338 (2010).
- [81] P. Corboz, R. Orús, B. Bauer, and G. Vidal, Simulation of strongly correlated fermions in two spatial dimensions with fermionic projected entangled-pair states, Phys. Rev. B 81, 165104 (2010).

- [82] E. J. Bergholtz and Z. Liu, Topological flat band models and fractional chern insulators, International Journal of Modern Physics B 27, 1330017 (2013).
- [83] S. A. Parameswaran, R. Roy, and S. L. Sondhi, Fractional quantum hall physics in topological flat bands, Comptes Rendus Physique 14, 816–839 (2013).

APPENDIX: LONG-RANGE DATA FOR D=3 SU(2)-INVARIANT PEPS

In this appendix we present the scaling analysis of data for D=3 SU(2)-invariant PEPS ansatz, employed in [61]. The real-space spin-spin correlations, scaling of the correlation length, and the leading part of the transfer matrix spectrum are presented in Fig. 6. The real-space spin-spin correlations show two distinct regimes analogous to the unrestricted PEPS ansatz: Up to a range of roughly 10 sites an exponential decay with $\xi_{\text{bulk}} = 0.54$ then crossing over into regime of extremely slow decay with strong finite- χ dependence. Crucially, the scaling of finite- χ correlation length is compatible with the second regime becoming genuine algebraic decay in the $\chi \to \infty$ limit. In particular, we scale finite- χ data in two different ways: First, by extracting the spin-spin correlation length ξ_{SS} from the tails of spin-spin correlations and performing a power-law fit with respect to the environment dimension χ . Second, by scaling the correlation length $1/\xi_{TM}$ given by the leading gap in the transfer matrix E against the subleading gap and again performing power-law fit as suggested by Ref. [70]. Note, that unlike in the case of unrestricted PEPS, i.e. for D=5 shown in the inset of Fig. 2, the order of the eigenvalues of E is not fixed. For large D^2/χ , the subleading eigenvalue λ_1 is two-fold degenerate but for $D^2/\chi \lesssim 0.1$ the subleading eigenvalue λ_3 is instead four-fold degenerate. Moreover, the data suggest that for larger D^2/χ the λ_7 will surpass the quadruplet and hence for the purpose of the scaling we use the subleading gap between λ_1 and λ_7 .

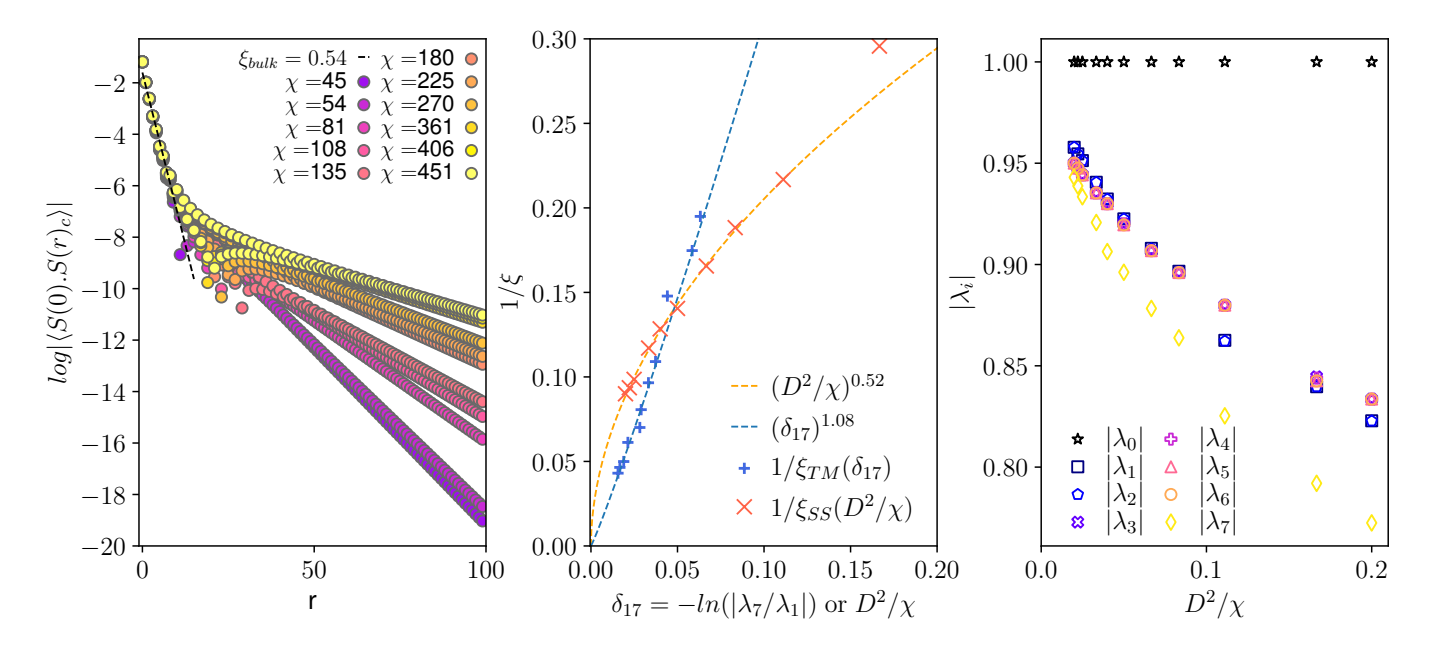


FIG. 6. Long-range properties of SU(2)-invariant D=3 iPEPS. Left: Connected part of the real space spin-spin correlation functions. Center: Scaling of the correlation length by subleading gap $\delta_{17}=-log|\lambda_7/\lambda_1|$ in the transfer matrix E. Right: Leading part of the transfer matrix spectrum as a function of environment dimension χ .